Plastic Deformation of Irradiated Zirconium Alloys: TEM Investigations and Micro-Mechanical Modeling

Fabien Onimus, J-L Bechade, Claude Prioul, Philippe Pilvin, Isabelle Monnet, Sylvie Doriot, Bénédicte Verhaeghe, Didier Gilbon, Laurence Robert, Laurent Legras, et al.

Onimus, F., Béchade, J.L., Prioul, C., et al., 2005. Plastic deformation of irradiated zirconium alloys: TEM investigations and micro-mechanical modeling. In Zirconium in the Nuclear Industry: Fourteenth International Symposium. ASTM International, (ASTM STP 1467). Journal of ASTM International, Vol. 2, No. 8, DOI: 10.1520/JAI12424

DOI: 10.1520/JAI12424

Journal of ASTM International, September 2005, Vol. 2, No. 8

Fabien Onimus,[1]* *Jean-Luc Béchade,*[1] *Claude Prioul,*[2] *Philippe Pilvin,*[3] *Isabelle Monnet,*[1] *Sylvie Doriot,*[1] *Bénédicte Verhaeghe,*[4] *Didier Gilbon,*[4] *Laurence Robert,*[5] *Laurent Legras,*[5] *and Jean-Paul Mardon*[6]

Plastic Deformation of Irradiated Zirconium Alloys: TEM Investigations and Micro-Mechanical Modeling

ABSTRACT: TEM investigations have been performed on irradiated samples after deformation covering various testing conditions for different recrystallized Zr alloys. It is shown that for transverse tensile tests and internal pressure tests performed at 350°C, only basal channels are observed for strain levels up to uniform elongation, whereas only prismatic and pyramidal channels are observed for axial tensile test. Then, focusing on internal pressure testing, irradiation hardening and strain hardening behavior have been analyzed in detail and compared to TEM observations. It is proposed that dislocation channeling phenomenon leads to high strain incompatibility between channels and surrounding grains and therefore to high microscopic internal stresses. These high microscopic internal stresses are believed to induce strong kinematic hardening at the macroscopic scale, as suggested by the mechanical behavior analysis. Finally, a micro-mechanical model based on microscopic deformation mechanisms and using homogenization techniques is proposed, taking into account the observed channeling phenomenon.

KEYWORDS: dislocation channeling, irradiation, loop, internal stress, zirconium alloy

Introduction

Zirconium alloys, mainly used as fuel cladding tubes in light water nuclear reactor, undergo fast neutron irradiation leading to strong irradiation damage. Since the cladding is the first confinement barrier of the radioactive material, it is essential to keep its mechanical integrity throughout its lifetime, especially under service conditions. Consequently, an important part of the research undertaken on these materials aims at increasing the knowledge of irradiation effects on mechanical properties and microstructure in order to develop a predictive model for irradiated Zr alloys. Lately a micro-mechanical model, based on homogenization theory and deformation mechanisms, has been developed [1,2] for non-irradiated material. Nevertheless, in order to extend this type of approach to irradiated zirconium alloys, the deformation mechanisms have to be clearly characterized and understood.

Manuscript received 15 March 2004; accepted for publication 23 February 2005; published September 2005. Presented at ASTM Symposium on Zirconium in the Nuclear Industry: Fourteenth International Symposium on 13–17 June 2004 in Stockholm, Sweden; B. Kammenzind and P. Rudling, Guest Editors.

[1] Research Engineer, CEA/DEN, Service de Recherches Métallurgiques Appliquées, CEA-Saclay, 91191 Gif-sur-Yvette Cedex, France.

[2] Pr., Ecole Centrale Paris, Laboratoire de Mécanique des Sols, Structures et Matériaux, 92295 Châtenay-Malabry, France.

[3] Pr., Université de Bretagne Sud – IUP Lorient, Laboratoire de Génie Mécanique et Matériaux, 56321 Lorient, France.

[4] Research Engineer, CEA/DEN, Service d'Etude des Matériaux Irradiés, CEA-Saclay, 91191 Gif-sur-Yvette Cedex, France.

[5] Research Engineers, Electricité de France, R&D Division, Materials and Mechanics of Components, Les Renardières, 77818 Moret sur Loing, Cedex, France.

[6] Consulting Engineer, Framatome-ANP Nuclear Fuel, 10 Rue Juliette Récamier, 69456 Lyon Cedex 06, France.

*Principal author to whom the correspondence should be addressed. E-mail: fabien.onimus@cea.fr.

It is known that neutron irradiation leads to a significant increase in strength and a strong reduction in uniform elongation with an associated highly localized necking as reviewed in [3]. From a microscopic point of view, it has been established that in zirconium alloys irradiation damage at low fluence [4] consists mainly in the formation of interstitial and vacancy <a> type prismatic loops, with prismatic habit planes. As reviewed by Bement [5] and Hirsch [6], the increase in strength observed in irradiated materials is usually attributed to the presence of the high density of small irradiation-induced loops which can act as obstacles against dislocation glide. However, these obstacles can be overcome by dislocations when a sufficient stress is applied; then the loops can be dragged by dislocations. This process of removal of irradiation loops produces a cleared zone free of defects inside the grain. These obstacle-free channels will therefore constitute preferred areas for further dislocation gliding, leading to plastic strain localization at the grain scale with regions of very high plastic strain surrounded by regions of almost zero plastic strain. This mechanism, called dislocation channeling, has been observed in many different irradiated materials as reviewed by Wechsler [7]. In the case of zirconium alloys, several authors have reported defect free channels [8–14], however, there is yet no agreement on the type of activated slip systems. Indeed, for transverse tensile test, Adamson [12] reported mainly prismatic and pyramidal channels for an irradiated high oxygen ([O] = 1400 ppm) Zr alloy, whereas Régnard [14] observed mainly basal channels and, to a lesser extent, pyramidal and prismatic channels, for irradiated recrystallized Zy-4. As a conclusion, it is worth noticing that there is no agreement between the different authors and that too few observations have been performed for other types of loading directions and testing conditions. It also has to be highlighted that the link between macroscopic mechanical behavior and dislocation channeling mechanism has rarely been investigated in detail [15]. In order to develop a predictive model based on deformation mechanisms, a more statistical characterization is necessary. It is also important to have a better understanding of the effect of test conditions, such as loading direction, strain rate, test temperature, and strain level, on deformation mechanisms.

The first part of this paper describes a Transmission Electron Microscopy (TEM) investigation of plastic deformation mechanisms in neutron irradiated recrystallized Zr alloys tested with different loading conditions. The second part of this paper analyzes the mechanical behavior for internal pressure test loading (at 350°C) in detail and compares the analysis to the TEM observations. Finally, a micro-mechanical model based on the observed deformation mechanism is proposed for the internal pressure test at 350°C.

Materials and Experimental Procedure

Materials and Mechanical Testing

In order to have a better insight into the mechanisms involved in plastic deformation of irradiated Zr alloys, numerous mechanical tests and TEM investigations have been performed on various recrystallized zirconium alloys specimens. The four materials (Table 1) used for this study are all recrystallized Zr alloys: Zy-4 (two different chemical compositions for sheet and cladding), M5™ alloy, and a previous experimental grade alloy called here Zr-1%Nb-O and referred to as M5-0 in [16]. These materials have been irradiated in different reactors (MRT and PWR), at various irradiation temperatures and up to various fluences (Table 2). This variability in irradiation conditions is assumed to be a second order effect in considering the deformation mechanisms.

TABLE 1—*Alloys chemical composition (weight %).*

Alloy	Sn	Nb	Fe	Cr	O	Zr
Zy-4 (sheet)	1.40	...	0.20	0.105	0.125	bal.
Zy-4 (cladding)	1.30	...	0.210	0.100	0.125	bal.
Zr-1 %Nb-O (cladding)	...	1.0	0.02	...	0.125	bal.
M5™ (cladding)	...	1.0	0.035	...	0.130	bal.

TABLE 2—*Materials, irradiation conditions, and test conditions of the specimens.*

Specimen	Material	Reactor	Fluence, n/m^2 (E>1 MeV)	Irradiation Temp.	Mechanical Test	Test Temp.	Strain Rate, s^{-1}
A	Zy-4 sheet	Siloé	0.6×10^{25}	280°C	Transverse tensile	350°C	1.6×10^{-4}
B	Zy-4 sheet	Siloé	0.6×10^{25}	280°C	Transverse tensile	350°C	1.6×10^{-4}
C	Zr-1%Nb-O cladding	PWR	12×10^{25}	350°C	Internal pressure	350°C	3×10^{-4}
D	Zy-4 cladding	Osiris	0.4×10^{25}	350°C	Internal pressure	350°C	3×10^{-4}
E	Zr-1%Nb-O cladding	PWR	12×10^{25}	350°C	Axial tensile	350°C	3×10^{-4}
F	Zy-4 cladding	Siloé	3.1×10^{25}	350°C	Ring tensile (interrupted)	350°C	1.6×10^{-4}
G	M5™ cladding	Siloé	2.4×10^{25}	380°C	Ring tensile (interrupted)	350°C	1.6×10^{-4}
H	M5™ cladding	PWR	3.5×10^{25}	350°C	Internal pressure (stress relaxation at *E*=0.8 %, 72 h)	350°C	3×10^{-4}
I	M5™ cladding	PWR	3.5×10^{25}	350°C	Internal pressure (stress relaxation at *E*=0.8 %, 72 h)	350°C	3×10^{-6}
J	M5™ cladding	PWR	3.5×10^{25}	350°C	Internal pressure (stress relaxation at *E*=0.8 %, 72 h)	400°C	3×10^{-6}
K	M5™ cladding	PWR	8×10^{25}	350°C	Internal pressure (creep at 300 MPa during 500 h)	350°C	-

After irradiation, different types of mechanical tests have been performed on these four materials: transverse tensile tests on rolled sheet, ring tensile tests ($\sigma_{\theta\theta}$) on rings machined out of tubes in a double dog-bone shape after irradiation [17], internal pressure tests ($\sigma_{\theta\theta}$, $\sigma_{zz}= \sigma_{\theta\theta}/2$) on tubes, and axial tensile tests (σ_{zz}) on tubes. All internal pressure tests have been performed using a dynamically controlled pressurization device. This is particularly important for the constant strain rate tests. The ring tests have been performed using the procedure described in [17]. In addition to the classical strain hardening tests, stress-relaxation tests (during 72 h) and creep test (during 500 h) were conducted using internal pressure loading. Stress-strain curves and strain-time curves are given in Figs. 6*a* and *b*. The irradiation and testing conditions of the eleven specimens studied here are given in Table 2. In addition to these data, it has to be pointed out that the textures of these materials are typical of recrystallized Zr alloy cladding or rolled sheet. It also has to be noticed that the A specimen was cut out from a 1-mm thick sheet in the TD-LD plane, whereas the B specimen was cut from a 10-mm thick sheet in the TD-ND plane. This last specimen is particularly interesting because it allows the investigation of the channel 3D structure.

TEM Procedure

After mechanical testing, all the thin foils were prepared in hot cell as described in [18]. In addition, on some thin foils a notch was left in order to know the orientation of the sample.

First, in order to confirm previous observations [8–14] and to identify precisely the activated slip systems according to the loading direction (transverse, internal pressure, and axial), a statistical TEM investigation was carried out on the five specimens listed in Table 2 (A–E, tested at 350°C). For each thin foil taken from these specimens, many grains were studied successively in arbitrary areas. The local orientation was determined by means of conventional diffraction pattern indexing in order to draw the stereographic projection for each grain. Examinations were carried out at relatively high magnification in order to determine whether grains contain channels, by tilting the specimen successively in the entire accessible angular domain (±45°, ±30°) of the double tilt sample holder. Then, in order to identify the channeling slip system, the traces of the channels were systematically analyzed on the stereographic projection. Moreover, the tilt conditions were recorded for the maximum contrast between channels and surrounding material. These conditions correspond to the situation where the channeling plane nearly contains the electron beam. These two complementary methods allow the channeling slip system to be determined without ambiguity especially in the case of basal channeling. Finally, the mean number of channels per grain and the mean channel width have been roughly characterized. Extended experimental details and results are given in [19].

In a second step, using similar procedures, the six other specimens listed in Table 2 (F–K) were studied qualitatively in order to extend the understanding of the deformation mechanisms to other testing conditions (strain rate, creep, temperature, strain level). TEM observations are shown schematically on Fig. 5*a* and Figs. 6*a* and *b*.

Results of TEM Investigations

Statistical TEM Analysis

Experimental Observations—On the two transverse tensile specimens (A and B), 81 grains have been studied. It has been observed that 38 grains over 81 contained basal channels (Fig. 1*a*). No other type of channel has been observed. The other 43 grains did not exhibit any sign of plastic deformation. On the C and D specimens tested in internal pressure loading, 80 grains have been studied, and 43 grains over 80 contained basal channels (Fig. 1*b*). As in the previous case, no other type of channel was observed. It has also to be underlined that for all of the A, C, and D specimens, connecting channels were very seldom observed (only two grains over 64 grains with basal channels observed), whereas on the B specimen many basal channels were connected from grain to grain (17 grains with connecting channels over 21 grains with basal channels). For all these four specimens, the width of the channels was always less than 100 nm, and the mean width was between 40 and 80 nm. It also has been estimated that there are on average 3–5 channels per grain. On specimen E, tested under uni-axial loading (axial tensile test), 41 grains have been studied, and 20 of these 41 grains contained prismatic and pyramidal channels, no basal channel was observed. In two cases, it has not been possible to distinguish between prismatic and pyramidal channels, however it has been determined that 14 grains contained prismatic channels, and 4 grains contained pyramidal channels as shown on Figs. 2*a* and *b*. In addition to that, it has to be noticed that the channels were more difficult to observe in this case and did not seem fully cleared of defects. The mean width of channels has been roughly estimated at 40 nm, the maximum width is 50 nm, and there are, on average, five channels per grain. All of these results are reported in Table 3.

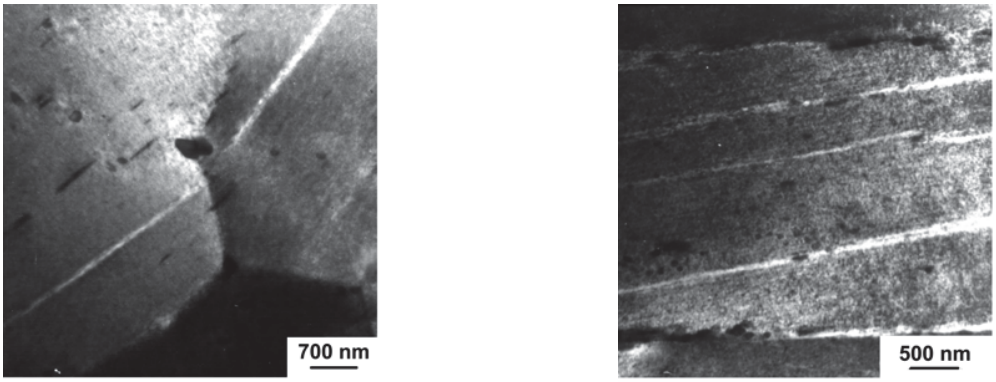

(a) (b)

FIG. 1—*(a) Propagating basal channels in B specimen and (b) basal channels in C specimen.*

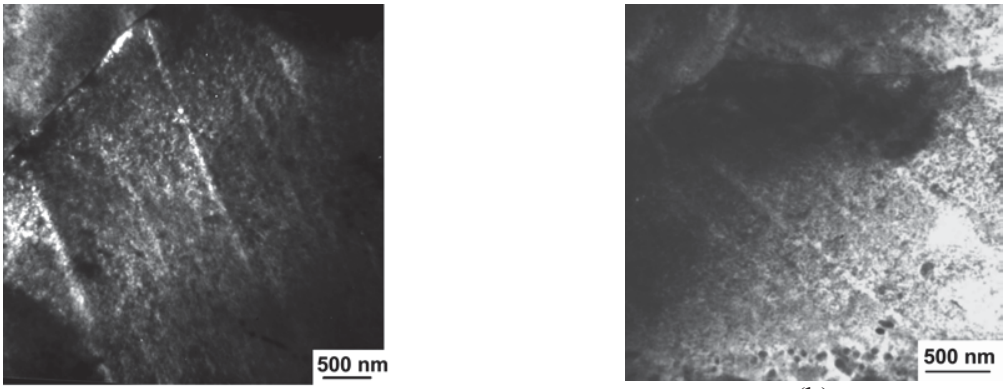

(a) (b)

FIG. 2—*(a) Prismatic and (b) pyramidal channels observed in E specimen.*

TABLE 3—*Results of the statistical TEM observations of the five different specimens.*

Specimen	Mechanical Test	E^p	Studied Grains	Grains with Channels	Channeling Plane
A	Transverse tensile	0.4 %	52	21	B
B	Transverse tensile	0.36 %	29	17	B
C	Internal pressure	0.5 %	47	28	B
D	Internal pressure	0.2 %	33	15	B
E	Axial tensile	1.6 %	41	20	P and π_1

Discussions—The TEM observations of the A, B, C, and D specimens lead to the conclusion that only basal channeling occurs at 350°C for transverse tensile test and internal pressure test and for plastic strain up to uniform elongation. This result has to be compared with the deformation mechanisms in non-irradiated material. Indeed, it has been established, as reviewed by Douglass [3] and Tenckhoff [20], that for low plastic strain, plastic deformation occurs essentially by <a> dislocations gliding on prismatic planes for axial, transverse, or closed end pressure loading. This is due to the fact that the Critical Resolved Shear Stress (CRSS) of the prismatic slip system is lower than that of the other slip systems. The important change in slip system activation with irradiation can be attributed to a modification in the hierarchy of the CRSS. This can be explained by the difference in the interactions between loops and dislocations, which implies that dislocation channeling is easier in the basal plane than in the prismatic plane. Indeed, as it has been proposed by Fregonese [13] and Régnard [14], the fact

that in the hexagonal closed packed structure (h.c.p.) all the <a> Burgers vectors lie in the basal plane implies that the junctions created between a <a> loop and a <a> dislocation gliding in the basal plane are always glissile. Therefore, the loops can be easily swept up by basal dislocations, which would lead to an easy dislocation channeling and to a low increase in the critical shear stress. On the contrary, in the case of a <a> dislocation gliding on the prismatic plane interacting with a <a> loop, the junction created is sessile in two out of three cases, which leads to a lower ability for dislocation channeling and therefore to a higher CRSS. This explanation also applies for pyramidal slip system.

However, we have seen that for an axial tensile test (E specimen), prismatic channeling and pyramidal channeling occur. This is due to the fact that since the material is characterized by a strong texture with the <c> axis tilted about 30° around the normal (or radial) direction in the TD-ND plane (r-θ plane), a large majority of the grains present a very low resolved shear stress on the basal plane for an axial tensile test. Therefore, in order to accommodate the plastic deformation, other slip systems, such as prismatic or pyramidal, must be activated for axial tensile test loading conditions. This can be achieved by the sweeping up of only one type of <a> loop or by another mechanism such as the one proposed by Carpenter [21]. Nevertheless, it is seen that the sweeping up of loops is limited for these slip systems since the channels do not seem to be fully cleared of defects.

The 3D structure of the basal channels has also been investigated thanks to the thin foils taken in the B specimen. Indeed, on the B specimen, propagation of channels from grain to grain has been observed for 11 grains out of 17 with basal channels, whereas in all other specimens (A, C, and D) this feature has only been observed for 2 grains out of 64 with basal channels. This can be explained by the fact that the propagation of channels from grain to grain occurs in the shearing direction. In this case, since the material exhibits a strong texture (<c> axis in the ND-TD or r-θ plane as shown on Fig. 3*a*), for internal pressure test and transverse tensile test, the best orientation for the shearing direction is contained in the ND-TD plane (or r-θ plane) and is tilted 45° from the normal direction. Therefore, in order to observe the propagation of grains, it is necessary to take the thin foil in the ND-TD plane (Fig. 3*b*), as proved by TEM investigations of the B specimen. On the contrary, if the thin foil is taken in the TD-LD plane (or z-θ plane), as in the case of A, C, and D specimens, the propagation of channels will be seldom observed in agreement with the TEM observations. The propagation of channels in surrounding grains is probably due to the high stress concentration on the grain boundary due to the strong plastic strain localization in the channel.

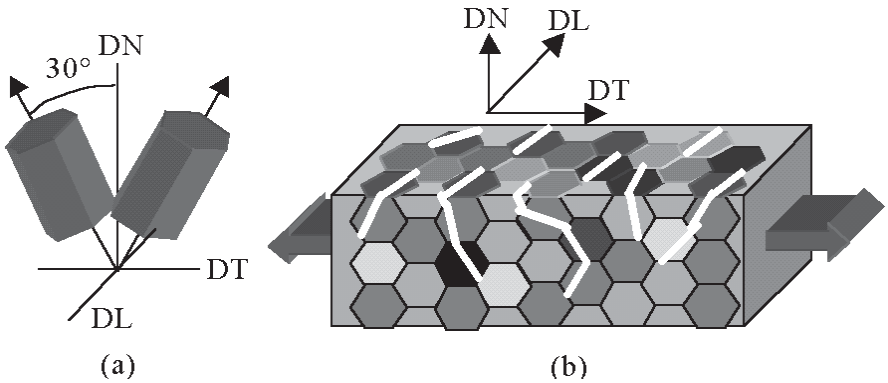

FIG. 3—*Schematic drawing describing the propagation of basal channels for a transverse tensile test: (*a*) Main grains orientation, (*b*) Propagation of channels in the specimen frame.*

All of these observations obtained for materials tested at 350°C, and for a strain rate of 3×10^{-4} s^{-1} show a good coherency and lead to a better understanding of the dislocation channeling mechanism in irradiated zirconium alloys. Nevertheless, in order to extend these conclusions to broader test conditions (test temperature, strain rate, plastic strain level, and creep), six other specimens have been studied.

Extending the Analysis to Different Loading Conditions

Effect of Stress Relaxation—On the H specimen, many basal channels have been observed as in the case of the C and D specimen as shown on Fig. 4*c*. This proves that the basal channels created during the strain hardening phase have not been affected by the stress relaxation phase performed during 72 h.

Effect of Strain Rate—Basal channels have also been observed in the I specimen tested under internal pressurization at 350°C and at a strain rate of 3×10^{-6} s^{-1} (Fig. 4*d*). These channels are similar to the channels observed for tests performed at 3×10^{-4} s^{-1} (C, D, H specimens). This proves that within this range of strain rate, the plastic deformation mechanism is not affected by the strain rate and occurs by basal channeling (before uniform elongation).

Effect of Creep—On the K specimen, a start of recovery of the irradiation microstructure has been noticed, after a creep test performed at 350°C and during 500 hours. A small decrease in <a> loops density seems to have occurred, probably assisted by stress, leading to homogeneously deformed areas, similar to non-irradiated materials. However, basal channels could still be observed in this specimen, as shown in Fig. 4*f*.

Effect of Test Temperature—On the J specimen, it has been observed that the irradiation microstructure has been partially annealed, showing larger loops than in the previous specimens. In this case, the plastic deformation seems to take place homogeneously since no channels but many dislocation lines are observed as shown on Fig. 4*e*. It is believed that these dislocations glide in the prismatic plane as in the case of non-irradiated material.

Effect of Plastic Strain Level—Thin foils have been taken in the gauge length of the F and G ring specimens, the test being interrupted after the load drop beyond the uniform strain limit, before failure, as shown on Fig. 1 reported in [14]. On these thin foils, many channels have been observed. However opposite to the observations on the A and B specimens studied in the first part, in this case, the channels correspond to the basal as well as to the pyramidal and the prismatic slip system as shown on Figd. 4*a* and *b*. This suggests that before uniform elongation, only basal channeling occurs, whereas for strain level higher than uniform elongation, other types of channels start to appear, probably due to the need to accommodate the plastic deformation in the necking zone.

The TEM results are summarized in Table 4, and the analysis is reported in Table 5. It has also to be underlined that only six specimens have been chosen here, but all of these observations have been confirmed on other specimens deformed in the same conditions.

Mechanical Behavior Analysis: Irradiation Induced Hardening and Strain Hardening Behavior

In order to understand the effect of dislocation channeling mechanism on the mechanical behavior of irradiated Zr alloys, the tests performed in internal pressure loading on the C, D, and H specimens, respectively, recrystallized Zy-4, Zr-1%Nb-O alloy, and M5™ alloy (tests

performed at 350°C, with a strain rate of 3×10^{-4} s^{-1}), presented above, have been analyzed in details. The analysis has been mainly focused on irradiation induced hardening and on the strain hardening behavior of irradiated material, also considering the TEM observations performed on the C, D, and H specimens. The cylindrical geometry of the internal pressure specimen allows very precise extensometry during the mechanical testing, therefore the mechanical behavior for this loading condition is known very accurately. Stresses and strains are computed for internal pressure tests by using the usual thin wall approximation (e.g., [22]).

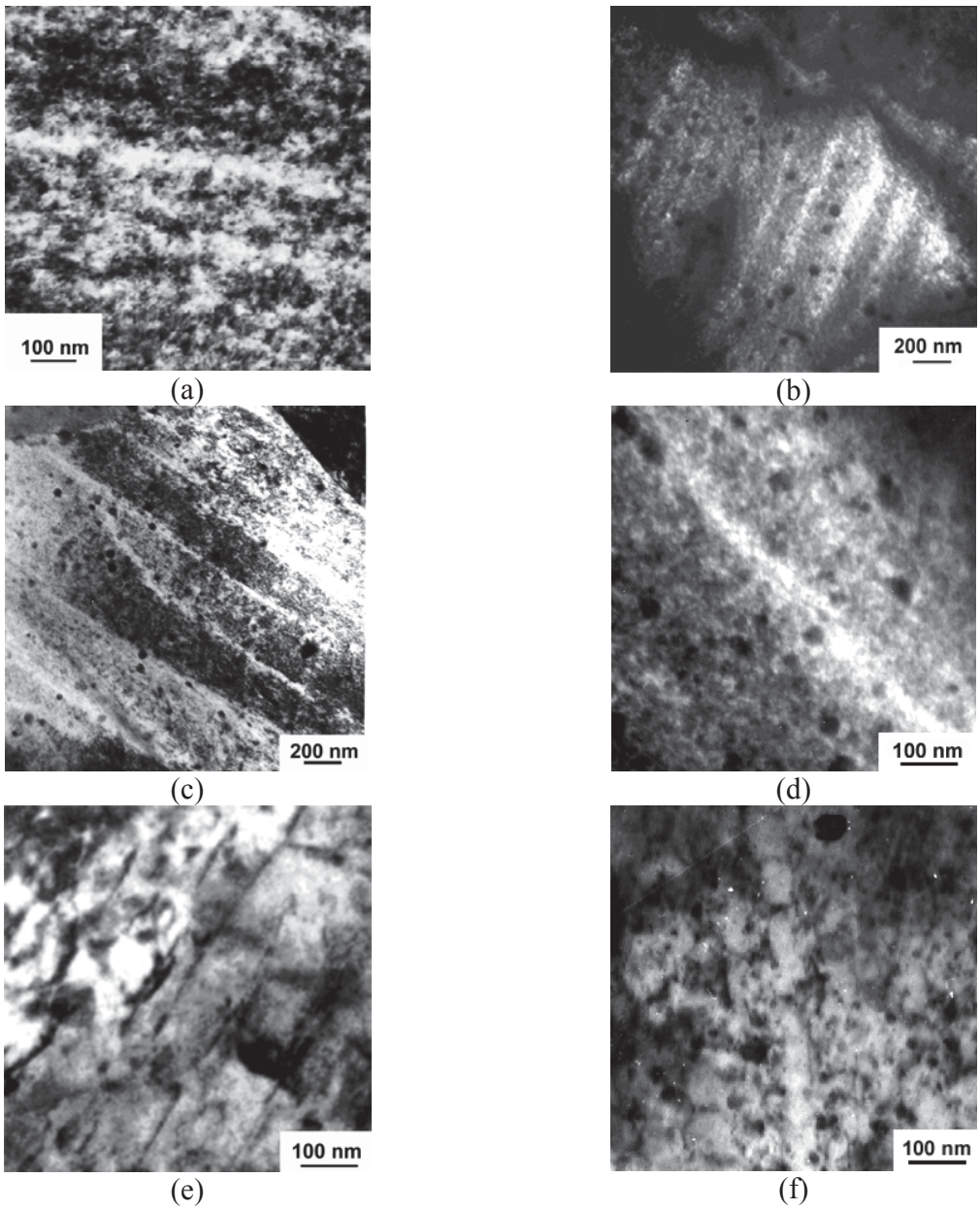

FIG. 4—*(a) Basal channels in the F specimen, (b) prismatic channels in the G specimen, (c) basal channels in the H specimen, (d) basal channel in the I specimen, (e) annealed irradiation microstructure, <a> dislocations probably gliding in prismatic planes in the J specimen, (f) partially annealed irradiation microstructure, basal channel in the K specimen.*

TABLE 4—*Results of the qualitative TEM observations of the different specimens.*

Specimen	Mechanical Test	Test Temperature	Strain Rate, s^{-1}	E^p %	Deformation Mechanism	Activated Slip System
F	Ring tensile	350°C	1.6×10^{-4}	6.7	channeling	B, π_1, P
G	Ring tensile	350°C	1.6×10^{-4}	7.4	channeling	B, π_1, P
H	Internal pressure (stress relaxation at E=0.8 %)	350°C	3×10^{-4}	0.25	channeling	B
I	Internal pressure (stress relaxation at E=0.8 %)	350°C	3×10^{-6}	0.3	channeling	B
J	Internal pressure (stress relaxation at E=0.8 %)	400°C	3×10^{-6}	0.33	homogeneous	B or π_1
K	Internal pressure (creep at 300 MPa during 500 h)	350°C	…	3.2	homogeneous and channels	B

TABLE 5—*Discussion on TEM observations obtained for various testing conditions.*

Effect	Specimens vs. Specimens	Conclusions
Strain rate (350°C)	I vs. H, C, D	No effect of strain rate between 3×10^{-6} s^{-1} and 3×10^{-4} s^{-1} for internal pressure test at 350°C.
Creep (350°C)	K vs. I, H, C, D	Start of recovery of irradiation microstructure. Basal channels and homogeneous deformation.
Temperature	J (400°C) vs. I (350°C)	Partial annealing of irradiation microstructure. Homogeneous deformation for test performed at 400°C, no channel observed.
Strain level (350°C)	F, G vs. A, B	For strain levels higher than uniform elongation, pyramidal and prismatic channels start to appear for transverse test (ring).

Results

Dimensional Measurements—Very accurate dimensional measurements, using laser imaging techniques, have also been performed on the D specimen in order to investigate the distribution of the plastic strain at the specimen scale. The profiles of the external diameter of the D specimen, obtained by the laser imaging technique, before and after testing show that the deformation is homogeneous in the zone where the thin foils have been taken, although at the grain scale the deformation is localized inside the channels.

Yield and Flow Stress—The stress-strain curves of the three specimens are reported on Fig. 5*a* and compared to non-irradiated materials for the same testing conditions. Thanks to the good sensitivity of the extensometers, the flow stress has also been plotted as a function of the plastic strain. This type of representation allows a much better insight into the stress-plastic strain behavior and therefore to the strain hardening behavior, as shown in Fig. 5*b*.

The TEM investigation has shown that channeling already occurs before 0.2 % plastic strain, therefore the flow stress at 0.2 % plastic strain does not correspond to the irradiation induced hardening due to the loops since these loops are already cleared up inside the channels. In order to estimate the hardening due to loops, it has been chosen to consider the flow stress at a very low plastic strain level (yield stress), say 0.005 % plastic strain. However, this stress is not known accurately ($\pm$20 MPa), since the elastic slop is not known precisely. The flow stress at 0.2 % plastic strain ($\sigma_{0.2\ \%}$) can thus be associated with the plastic flow occurring inside the channels. These data are reported in Table 6 and plotted as a function of the fluence in Fig. 7.

As reported by many authors [3,23–25], it is shown that irradiation leads to a strong increase in flow stress. It can be noticed on Fig. 7 that the flow stress as well as the yield stress saturates as the fluence increases, considering that all the different materials are equivalent to a first order.

It can also be noticed that for a non-irradiated material, the difference between yield and flow stress is low (of the order of 50 MPa), whereas once the material is irradiated, the difference between flow stress and yield stress is very high (of the order of 190 MPa). This shows that the strain hardening is higher for irradiated material than for non-irradiated material.

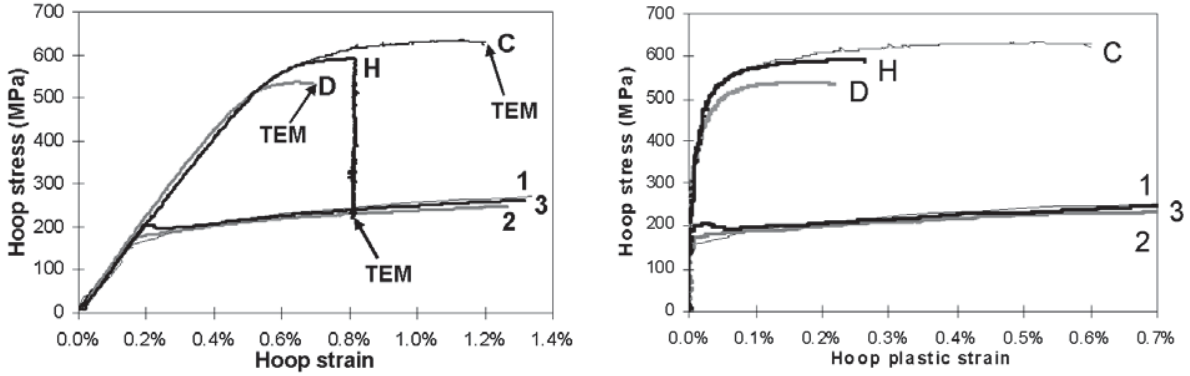

FIG. 5—*Internal pressure tests on C, D, and H specimens and compared to non-irradiated materials (1, 2, 3):* (a) *stress-strain curves,* (b) *stress-plastic strain curves. (Only the strain hardening phase is represented in the case of the H specimen on Fig. 5*b*).*

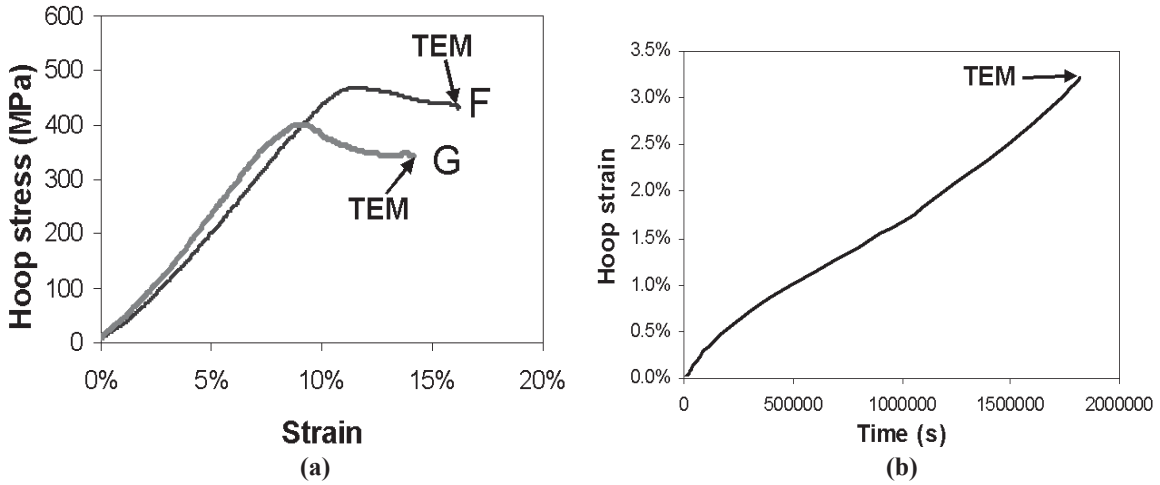

FIG. 6—*(*a*) Ring tests performed on the F and G specimens; (*b*) creep test performed on the K specimen.*

TABLE 6—*Flow stress for 0.005 % and 0.2 % of plastic strain for different materials and test conditions (irradiated materials compared to non-irradiated materials).*

Specimen	Material	Mechanical Test	Test Temperature	Strain Rate; s^{-1}	$\Sigma_{0.005\%}$, MPa	$\Sigma_{0.2\%}$, MPa
1	Zr-1%Nb-O	Internal pressure	350°C	3×10^{-4}	150	210
2	Zy-4	Internal pressure	350°C	3×10^{-4}	150	200
3	M5™	Internal pressure	350°C	3×10^{-4}	170	200
C	Zr-1%Nb-O	Internal pressure	350°C	3×10^{-4}	280	575
D	Zy-4	Internal pressure	350°C	3×10^{-4}	270	540
H	M5™	Internal pressure (stress relaxation at E=0.8 %)	350°C	3×10^{-4}	300	590

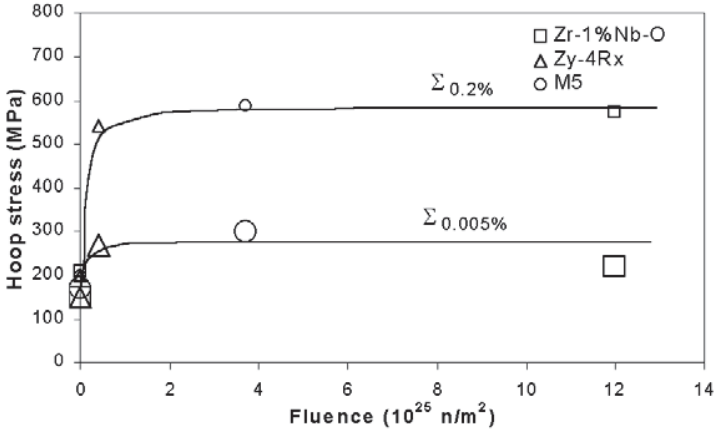

FIG. 7—*Evolution of yield stress and flow stress with irradiation fluence (n/m^2 E>1 MeV).*

Strain Hardening Rate—In order to investigate more accurately the strain hardening behavior of irradiated materials, the strain hardening rate has been computed for the mechanical test performed on the D specimen and compared to non-irradiated material. The strain hardening rate is plotted as a function of the stress as reported on Fig. 8. It is shown that the strain hardening rate is two orders of magnitude higher in irradiated material ($d\sigma/d\varepsilon^p \approx 1000$ GPa) than in non-irradiated material ($d\sigma/d\varepsilon^p \approx 10$ GPa) at the onset of the plastic flow. However, for irradiated material, the strain hardening rate decreases rapidly to values of the same order of magnitude as in non-irradiated material ($d\sigma/d\varepsilon^p \approx 10$ GPa), whereas for non-irradiated material, the hardening rate decreases slowly.

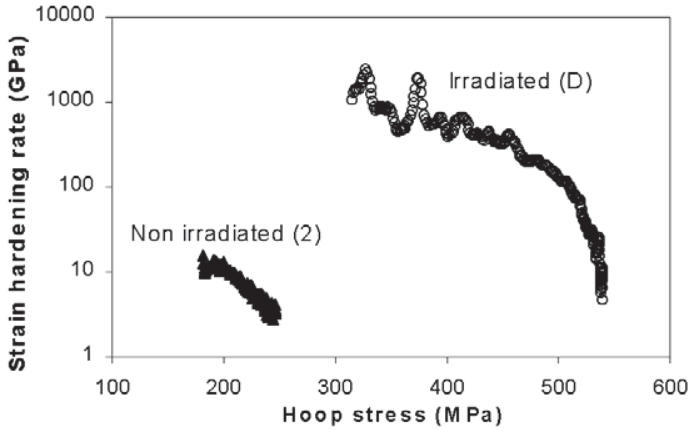

FIG. 8—*Strain hardening rate versus hoop stress for the internal pressure test performed on irradiated Zy-4 (D specimen) compared to non-irradiated material (2 specimen).*

Discussion on Mechanical Behavior Considering TEM Observations

It has been shown that irradiation leads to a strong hardening, as illustrated on Fig. 5 for yield stress ($\sigma_{0.005\ \%}$) and flow stress at 0.2 % ($\sigma_{0.2\ \%}$). The increase of the yield stress ($\sigma_{0.005\ \%}$) with irradiation can be directly related to the high loop density induced by irradiation. Indeed, according to the classical dispersed barrier hardening model reviewed by Refs. [5,6,26], dislocation loops act as obstacles against dislocation glide. However, when a sufficient shear

stress is applied, dislocations can overcome or sweep up all the obstacles encountered in the slip planes and macroscopic plastic deformation occurs. This stress level defines the macroscopic yield stress, which has been chosen in our case as the flow stress at very low plastic strain (0.005 % plastic strain).

The mechanical analysis also shows that the flow stress at 0.2 % plastic strain is increased by irradiation. However, in this case, TEM investigations of the D specimen have shown that for 0.2 % plastic strain, basal channels are observed. Since inside the channels irradiation loops have been cleared up by gliding dislocations, leaving the following dislocations with a defect free zone, it is surprising that irradiation hardening is still observed for this plastic strain level. In addition to that, it is seen on Fig. 5*b* that for the C specimen the flow stress increases between 0.2 and 0.5 % of plastic strain, and many channels can be observed for 0.5 % plastic strain. Assuming that for the C specimen channels were already present in the material at 0.2 % plastic strain as for the D specimen, it is also surprising that the flow stress increases since dislocation channeling corresponds to irradiation defects clearing, and therefore to local softening inside the channels. This phenomenon can be explained by considering the polycrystalline aspect of the material. Indeed, the strong localization of the plastic strain inside a channel leads to high strain incompatibility between the channel and the surrounding grains, which should induce elastic stress in return or microscopic internal stress. In addition, since only basal channeling occurs for the internal pressure test (only two independent deformation modes), compatibility conditions between grains cannot be satisfied. This phenomenon should also induce microscopic internal stress. These microscopic internal stresses are associated, at the macroscopic scale, to the kinematic hardening component of the flow stress or back stress. Therefore, in the case of irradiated material one would expect a strong kinematic hardening to occur because of the strong plastic strain localization inside the channels and the occurrence of only basal channeling. This high kinematical hardening could then balance the local softening inside the channel, leading to a hardening behavior at the macroscopic scale as observed for the C specimen. This would therefore explain that the plastic deformation at the specimen scale is still homogeneous, according to laser measurements, although at the grain scale, the plastic deformation occurs in a localized manner through dislocation channeling.

The high strain hardening rate measured at the onset of plastic flow in the case of irradiated material can also be interpreted as being a consequence of the localization of the plastic strain at the grain scale. Indeed, if a channel embedded into an elastic media is considered, for a small amount of macroscopic plastic strain, a high amount of plastic strain inside the channels is needed since it is assumed that all the plastic strain takes place inside the channels. Therefore, this high amount of local plastic strain will lead to a high increase of internal stress, thus leading to a high macroscopic strain hardening rate.

However, it is shown that the strain hardening rate decreases very rapidly in the case of irradiated material (Fig. 8) compared to non-irradiated material. The decrease of the strain hardening rate can be mainly attributed to the fact that the channels propagate from grain to grain due to the strong stress concentration at the grain boundaries, at the edge of the channels. This very low macroscopic strain hardening rate, due to channel propagation, would then induce strain localization at the specimen scale, which therefore can explain the strong decrease in uniform elongation with irradiation reported by many authors [3,23,27].

An extended analysis conducted on a larger data base (analysis of specimen unloading behavior, strain rate sensitivity, and stress relaxation), which will not be presented here, has also given some more clues that internal stress is actually higher for irradiated material than for non-

irradiated material. By using only the internal pressurization tests, it has not been possible to measure the internal stress level. Additional tensile-compression tests in the transverse direction are necessary to measure internal stresses for the transverse tensile direction.

Micromechanical Modeling for Internal Pressure Test Loading

On the basis of TEM investigations and mechanical behavior analysis, a micromechanical model has been developed for irradiated zirconium alloys. Starting from the dislocation scale, the dislocation-loop interaction has been modeled in a simple manner. Then the channel microstructure has been schematically described at the grain scale in order to model the macroscopic behavior of irradiated polycrystalline Zr alloys by means of homogenization techniques. Only internal pressure tests performed at 350°C have been modeled. Since only basal channeling has been observed in this case, only basal glide is taken into account. A table of mathematical symbols used is given in Table 7.

Modeling at the Dislocation Scale

Hardening—It is known that the high density of <a> loops act as obstacles against dislocation glide, in the same way as the forest dislocations. According to the classical dispersed barrier hardening model [5,6,26], the hardening phenomenon can be taken into account by adding a term, proportional to the square root of the loop density (N), to the critical resolved shear stress leading to the expression (Eq 1) for the basal critical shear stress, where α_i is the obstacle force, μ the shear modulus, b the Burgers vector, d the mean loop diameter and τ_0^B the critical resolved shear stress for the basal plane when the material is not irradiated.

$$\tau_\mu = \tau_0^B + \alpha_i \mu b \sqrt{Nd} \tag{1}$$

Softening—It has been shown that when a dislocation gliding on the basal plane interacts with <a> loops, glissile junctions are created, and the loop can be swept up on its cylinder, leading to clearing up of irradiation loops inside a band of the grain and therefore to local softening. The clearing up process can be modeled, as proposed by Rodney [28] and Pokor [29], by considering that all the loops lying within a distance H/2 to the dislocation plane (basal plane in this case) are captured and cleared up by the dislocation. Taking into account the dislocation density ρ inside the channel gliding at the velocity $\bar{v}$, it is shown that during a time dt, the number of cleared loops inside the channel is NHρvdt. Since the plastic strain rate $\dot{\gamma}$ inside the channel (microscopic strain rate) is related to the dislocation density inside the channel and to the dislocation mean velocity by the Orowan equation ($\dot{\gamma} = \rho b \bar{v}$), the number of loops cleared up inside the channel during the time dt can be expressed as $\frac{H}{b} N \dot{\gamma} dt$. Therefore, the equation governing the evolution of the loop density can be deduced, written here (Eq 2) in a more general way by adding the contribution of all the dislocations gliding on the three basal slip systems ($s \in B$).

$$\dot{N} = \frac{H}{b} N \sum_{s \in B} \left| \dot{\gamma}_s^{ch} \right| \tag{2}$$

TABLE 7—*Symbols used in the description of the model.*

τ_s	Resolved shear stress on the system s
$\tau^B{}_0$	Basal system critical resolved shear stress for non-irradiated material
τ_μ	Effective athermal critical shear stress for irradiated material
N	Loop density
d	Loop diameter
α_i	Obstacle force for irradiation induced loops
μ	Shear modulus
b	Burgers vector
ρ	Dislocation density
H	Annihilation distance
$\dot{\gamma}$	Shear strain rate
$\dot{\gamma}_0$	Reference shear strain rate
V_B	Basal activation volume
k	Boltzmann constant
$\underline{\underline{\mu}}_s$	Orientation two order tensor
$\underline{\underline{\Sigma}}$	Macroscopic stress
$\underline{\underline{\sigma}}_{ch}$	Stress inside the channel
$\underline{\underline{\varepsilon}}_{ch}$	Strain inside the channel
$\underline{\underline{\varepsilon}}^p_{ch}$	Plastic strain inside the channel
$\underline{\underline{\sigma}}_{outside}$	Stress outside the channel, inside the grain
$\underline{\underline{\sigma}}_g$	Stress inside the grain
$\underline{\underline{\varepsilon}}_g$	Strain inside the grain
$\underline{\underline{\varepsilon}}^p_g$	Plastic strain inside the grain
$\underline{l}_s$	Gliding direction
$\underline{n}_s$	Normal direction of slip plane
C	Four order elastic modulus tensor
S_{ch}	Eshelby four order tensor
I	Identity four order tensor
f_{ch}	Volume fraction of channels per grain
n_{ch}	Number of channels per grain
d_{ch}	Channel mean width
f_g	Volume fraction of grain
d_g	Grain size
γ_c	Critical value of shear for multiplication of channels
$\underline{\underline{\beta}}_{ch}$	Empirical effective plastic strain inside the channel

Thermally Activated Flow Law—The plastic strain rate inside the channel is given by the constitutive flow law, which is related to the thermally activated motion of dislocations. According to Refs. [30,31], the plastic strain rate can be expressed, if reverse motion is taken into account, as Eq 3, where τ_s is the applied resolved shear stress on the basal system s ($s \in B$)

inside the channel, τ_μ is the basal critical (athermal) resolved shear stress which takes into account the hardening due to irradiation induced loops, V_B is the basal activation volume, and $\dot{\gamma}_0$ is a coefficient which includes mobile dislocation density and lattice vibration characteristic frequency.

$$\dot{\gamma}_s^{ch} = \dot{\gamma}_0 \sinh\left(\frac{V_B Max\left(0,|\tau_s| - \tau_\mu\right)}{kT}\right) sign\left(\tau_s\right) \tag{3}$$

The applied resolved shear stress inside the channel is here computed as Eq 4, where $\underline{\underline{\mu}}_s$ is the two order orientation tensor of the considered slip system defined as given in Eq 5, where $\underline{l}_s$ and $\underline{n}_s$ are unitary vectors corresponding respectively to the shearing direction and to the normal of the slip plane.

$$\tau_s = \underline{\underline{\sigma}}_{ch} : \underline{\underline{\mu}}_s \tag{4}$$

$$\underline{\underline{\mu}}_s = \frac{1}{2}\left(\underline{l}_s \otimes \underline{n}_s + \underline{n}_s \otimes \underline{l}_s\right) \tag{5}$$

Modeling at the Grain Scale

Shape, Orientation, and Channel Volume Fraction—At the grain scale the specific channel microstructure has been schematically modeled as an oblate spheroid embedded into a spherical grain (Fig. 9). The thickness of this penny shaped ellipsoid corresponds to the width of the channel d_{ch}. Since only basal channels are taken into account, the short dimension d_{ch} of the flat ellipsoid corresponds to the <c> axis of the h.c.p. crystallographic structure and the plane of the flat ellipsoid corresponds to the basal plane. Homogeneous isotropic elasticity is also assumed. Considering a spherical shaped grain, the diameter of the channel corresponds to the diameter of the grain d_g. This very simple geometry allows Eshelby calculations for an ellipsoidal inclusion with uniform eigenstrain to be applied. Indeed, it has been shown by [32,33] that the stress inside the inclusion for an oblate spheroid embedded into an infinite elastic matrix, with macroscopic applied stress $\underline{\underline{\Sigma}}$ and eigenstrain inside the channels $\underline{\underline{\varepsilon}}_{ch}^p$, is given in Eq 6 where $\boldsymbol{C}$ is the four order elastic modulus tensor, $\boldsymbol{S_{ch}}$ is the Eshelby four order tensor for an oblate spheroid [32,33], I is the identity four order tensor, and $\underline{\underline{\varepsilon}}_{ch}^p$ is the plastic strain inside the channel.

$$\underline{\underline{\sigma}}_{ch} = \underline{\underline{\Sigma}} - C : (I - S_{ch}) : \underline{\underline{\varepsilon}}_{ch}^p \tag{6}$$

It has to be underlined that homogeneous and isotropic elasticity are also assumed for this modeling. Equation 6 is referred here as the concentration rule. Since it is assumed that all the plastic deformation of the grain is localized into the channels, the plastic strain of the grain, $\underline{\underline{\varepsilon}}_g^p$, is given by Eq 7, where f_{ch} corresponds to the volume fraction of channels per grain and $\underline{\underline{\varepsilon}}_{ch}^p$ to the mean plastic deformation inside the channels.

$$\underline{\underline{\varepsilon}}_g^p = f_{ch} \underline{\underline{\varepsilon}}_{ch}^p \tag{7}$$

This volume fraction can be very simply defined as Eq 8, assuming roughly a rectangular shaped channel and grain. In this expression, n_{ch} is the mean number of channels per grain, d_{ch} is

the mean width of channels, and d_g corresponds to the size of the equiaxed grain. V_g and V_{ch} account for the volume of the grain and for the volume of the channels, respectively.

$$f_{ch}=\frac{n_{ch}V_{ch}}{V_g}\approx\frac{n_{ch}d_{ch}}{d_g} \tag{8}$$

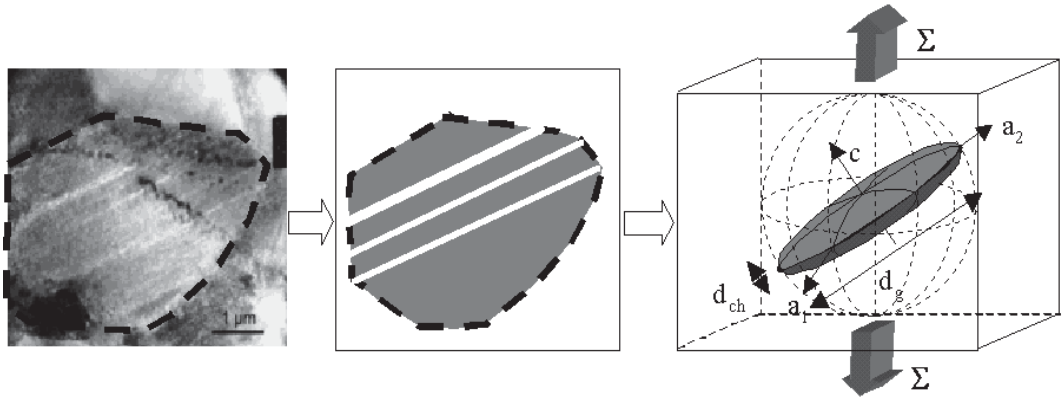

FIG. 9—*Schematic modeling of the channeling process. Basal channels are described as flat ellipsoid.*

It can be noticed that the concentration rule (Eq 6) actually describes the microscopic internal stress created by the localization of plastic strain inside the channels. Indeed, for a low plastic strain inside the grain ($\underline{\underline{\varepsilon}}^p_g$), the plastic strain inside the channel ($\underline{\underline{\varepsilon}}^p_{ch}$) is large, since the volume fraction of channels is of the order of 1–2 %. Therefore, although inside the channel the flow stress is low because of the clearing of loops, at the macroscopic scale, the flow stress is high due to the second term of Eq 6.

Knowing the shear strain rate on each basal slip system ($\dot{\gamma}_s$), the plastic strain rate inside the channels can be computed as Eq 9, taking into account the orientation of the grain with respect to the macroscopic orientation of the specimen. The plastic strain rate of the grain is then deduced by differentiating Eq 7.

$$\dot{\underline{\underline{\varepsilon}}}^p_{ch}=\sum_{s\in B}\dot{\gamma}_s\underline{\underline{\mu}}_s \tag{9}$$

Homogenization techniques do not aim at describing all the individual grains inside the representative volume of the polycrystalline material. With the homogenization techniques, only the grains having different crystallographic orientation are treated independently. Therefore, it is here considered that the sphere actually represents all the grains with the same crystallographic orientation, given by Euler's angles (ϕ_1, Φ, ϕ_2), and characterized by the volume fraction of grains with the same crystallographic orientation (f_g) obtained by X-ray diffraction texture analysis. The oblate spheroid inclusion inside the sphere therefore represents all the channels of all the grains with the same crystallographic orientation, characterized by the mean volume fraction of channels per grain with the same orientation (f_{ch}).

Channels Volume Fraction Evolution—The creation and multiplication of channels with plastic deformation is closely linked to the increase of the internal stresses with local plastic deformation. Indeed, it can be considered that when a critical level of internal stress for one

channel is reached, the channel will stop to deform, and another channel will be created inside the grain. For an isolated channel inside an infinite elastic matrix, the internal stress increases linearly with the local plastic strain, as shown in Eq 6. Therefore, for a critical value of plastic deformation inside the channel, let's say γ_c, the channel will stop to deform, and another channel will be created. As a consequence, the total plastic strain γ_{ch} due to n_{ch} channels, can be written as $\gamma_{ch}=n_{ch}\gamma_c$. Then, according to its definition, the evolution of the volume fraction of channels (f_{ch}) can be expressed as a function of the total plastic strain in all the channels of the grains with the same crystallographic orientation as in Eq 10, where the contributions of the three basal slip systems are added.

$$f_{ch}=\frac{d_{ch}}{d_g}\frac{1}{\gamma_c}\sum_{s\in B}\left|\gamma_s^{ch}\right| \tag{10}$$

Modeling at the Polycrystal Scale

In order to deduce the macroscopic behavior from the knowledge of the microscopic behavior, a polycrystalline model, developed by Pilvin [34] and Geyer [1], has been adapted to irradiated material. According to this approach, the calculation occurs in four successive stages for each time step. First, the macroscopic stress ($\underline{\underline{\Sigma}}$) is computed from the applied loading. Then, the stress inside the channel ($\underline{\underline{\sigma}}_{ch}$) is calculated by using the concentration rule. The plastic strain rate inside the channel ($\dot{\underline{\underline{\varepsilon}}}^{p}_{ch}$) is then computed thanks to the constitutive laws, and finally the macroscopic plastic strain rate ($\dot{\underline{\underline{E}}}^{p}$) is deduced from the computed microscopic plastic strain rate. However, in order to take into account the morphology of the channels in the case of irradiated material, the self-consistent computation described in [1,34] cannot be performed. This involves the use of a simplified approach as described below.

Loading Computation—From the macroscopic loading given in a mixed manner (stress and strain), the macroscopic stress is computed by using Hooke's law, assuming homogeneous isotropic elasticity (Eq 11) with the isotropic elastic modulus tensor defined as Eq 12, the behavior of the material being elasto-visco-plastic.

$$\underline{\underline{\Sigma}}=C\left(\underline{\underline{E}}-\underline{\underline{E}}^{p}\right) \tag{11}$$

$$C=2\mu\left(I-\frac{\nu}{1-2\nu}\underline{\underline{1}}\otimes\underline{\underline{1}}\right) \tag{12}$$

Stress Concentration Rule—Thanks to the concentration rule, the stress inside the channels can be computed, knowing the macroscopic applied stress. However, since the channels can propagate from grain to grain, the assumption that the channels can be considered as an ellipsoid embedded into an infinite elastic matrix cannot hold anymore. In order to take into account the channel propagation, the plastic strain inside the channels is replaced by a local effective plastic strain called $\underline{\underline{\beta}}_{ch}$, as shown in Eq 13. This semi-empirical effective plastic strain $\underline{\underline{\beta}}_{ch}$ evolves non linearly with the plastic strain ($\underline{\underline{\varepsilon}}^{p}_{ch}$), given by Eq 14, taking into account, in a simple manner, the plastic strain accommodation of the surrounding grains due to channel propagation

from grain to grain. Indeed, as the plastic strain inside the channel ($\underline{\underline{\varepsilon}}^{p}_{ch}$) increases, the effective strain ($\underline{\underline{\beta}}_{ch}$) saturates, leading to the saturation of the microscopic internal stresses which takes into account that the surrounding material does not behave elastically anymore. This effective strain $\underline{\underline{\beta}}_{ch}$ has no physical reality, the plastic strain in the channel is $\underline{\underline{\varepsilon}}^{p}_{ch}$. The third term added in Eq 14 takes also into account the static recovery of this effective plastic strain $\underline{\underline{\beta}}_{ch}$ especially useful for stress relaxation tests.

$$\underline{\underline{\sigma}}_{ch}=\underline{\underline{\Sigma}}-\underline{\underline{\underline{\underline{C}}}}:\left(\underline{\underline{I}}-\underline{\underline{\underline{\underline{S}}}}_{ch}\right):\left(\underline{\underline{\beta}}_{ch}-\frac{1}{f_{ch}}\underline{\underline{B}}\right) \tag{13}$$

$$\dot{\underline{\underline{\beta}}}_{ch}=\dot{\underline{\underline{\varepsilon}}}^{p}_{ch}-D\underline{\underline{\beta}}_{ch}\left\|\dot{\underline{\underline{\varepsilon}}}^{p}_{ch}\right\|-M\left(\left\|\underline{\underline{\beta}}_{ch}\right\|\right)^{m}\underline{\underline{\beta}}_{ch} \tag{14}$$

In addition to this, another term, called image stress by Mura [33], is added to stress concentration rule (Eq 13) in order to satisfy that the macroscopic stress equals the mean value of the microscopic stresses (Eq 15).

$$\underline{\underline{\Sigma}}=\sum_{g\in G}f_g\underline{\underline{\sigma}}_{g} \tag{15}$$

However, in order to satisfy this last condition, several assumptions have to be made. First, it is necessary to know the value of the stress in the grain outside the channels. Here, a simple assumption is made that outside the channels, the stress is of the order of the macroscopic applied stress (Eq 16).

$$\underline{\underline{\sigma}}_{outside}=\underline{\underline{\Sigma}} \tag{16}$$

Then, in order to satisfy the condition on the average of the stress (Eq 15), the two order tensor $\underline{\underline{B}}$ (in Eq 13) is defined as Eq 17.

$$\underline{\underline{B}}=\left[\sum_{g\in G}f_g\underline{\underline{\underline{\underline{C}}}}:\left(\underline{\underline{I}}-\underline{\underline{\underline{\underline{S}}}}_{ch}\right)\right]^{-1}:\left[\sum_{g\in G}f_g f_{ch}\underline{\underline{\underline{\underline{C}}}}:\left(\underline{\underline{I}}-\underline{\underline{\underline{\underline{S}}}}_{ch}\right):\underline{\underline{\beta}}_{ch}\right] \tag{17}$$

This simplified approach, although interesting, would require further improvements by using a self-consistent scheme such as the one developed in [1,2,34–37] in order to avoid the difficult introduction of the image stress as pointed out in [33]. Nevertheless, this is only possible if the morphology of the channels is not taken into account.

Macroscopic Plastic Strain Computation—Since the average of the microscopic strain is equal to the macroscopic strain (Eq 18), and assuming homogeneous elasticity, it can be shown that the macroscopic plastic strain is equal to the average of the microscopic plastic strain (Eq 19).

$$\underline{\underline{E}}=\sum_{g\in G}f_g\underline{\underline{\varepsilon}}_{g} \tag{18}$$

$$\underline{\underline{E}}^{p}=\sum_{g\in G}f_g\underline{\underline{\varepsilon}}^{p}_{g} \tag{19}$$

Assuming that no plastic strain occurs outside the channels ($\underline{\underline{\varepsilon}}^{p}_{outside}=0$), it is shown that the macroscopic plastic strain can be expressed as Eq 20.

$$\underline{\underline{E}}^{p}=\sum_{g\in G} f_g f_{ch} \underline{\underline{\varepsilon}}^{p}_{ch} \tag{20}$$

For each time step, all these formulas are computed for each grain (all grains with the same orientation), leading to the calculation of the macroscopic mechanical behavior by integrating constitutive laws at the grain scale. A file containing 240 orientations (ϕ_1, Φ, ϕ_2, f_g), representative of the texture of the zirconium alloys of the cladding is used. The slip system geometry and the orientation of the ellipsoids are explicitly taken into account in the modeling.

Results

The modeling includes several coefficients and parameters that have to be adjusted based either on TEM observations, microscopic data, or macroscopic results. First, a fitting of the non-irradiated modeling has been performed on non-irradiated M5 according to the approach described in [1,34], but this is not presented here. For non-irradiated material, coefficients for prismatic, basal, and first order pyramidal (<a> and <c+a>) slip systems are fitted. The coefficients obtained for non-irradiated material such as elastic coefficients (μ = 28.6 GPa, ν = 0.4), reference strain rate ($\dot{\gamma}_0 = 10^{-10}$ s^{-1}), basal critical shear stress (τ_B = 40 MPa), and basal activation volume ($V_B = 60b^3$), are given in Table 7. Only the coefficient for basal slip system are given here since for irradiated material tested in internal pressure test only basal systems are activated. These coefficients are in agreement with the data given in the literature [38–40].

Then, several coefficients have been chosen according to TEM examinations, such as the initial loop density before straining ($N_0 = 5 \times 10^{22}$ m^{-3}), the mean loop diameter (d = 8 nm), the mean grain size (d_g = 8 μm), and the mean width of the channels (d_{ch} = 210 nm). The value chosen here for the mean width of the channels is larger than the actual observed width so as to have a better description of the strain hardening at the onset of plastic flow. The rate of channel increase, given by γ_c, is adjusted in order to obtain a good order of magnitude fit for the channel volume fraction ($f_{ch} \approx 2$ %). It is also considered that the capture distance is equal to the loop diameter ($H = d$ = 8 nm). The obstacle force is also chosen according to literature data. In this case, since the created junctions are glissile in the basal plane, the obstacle force is relatively weak. The value chosen here is $\alpha_i = 0.1$.

Finally, the fitting for irradiated material has been performed on an extended data base taking into account various strain rates (3×10^{-4} s^{-1} to 3×10^{-6} s^{-1}) and stress relaxation tests but only for internal pressure tests performed at 350°C. The values for the coefficients chosen and the three fitting parameters obtained are given in Table 8. Only three empirical fitting parameters are used here (D, M, m). These three empirical parameters can be related to physical phenomenon. The D parameter is related to the plastic accommodation of the surrounding grains, and the M and m parameters are related to the visco-plastic accommodation of the surrounding grains, leading to static recovery of internal stresses. The apparent channels mean width has been previously adjusted in order to obtain a good description of the strain hardening rate at the onset of plastic flow. This coefficient indeed has a significant effect on the strain hardening rate at the onset of plastic flow. The agreement between simulation and experimental results is illustrated in Fig. 10. It has to be underlined that contrary to the non-irradiated approach, no self consistent calculations are made in this case, the empirical fitting parameters D, M, and m being adjusted on the macroscopic behavior.

TABLE 8—*Coefficients and parameters of the modeling.*

Coefficients adjusted on non-irradiated material					Microscopic coefficients obtained from TEM observations and literature results							Fitting parameters		
Y, MPa	ν	τ_B, MPa	V_B b^3	$\dot{\gamma}_0$ s^{-1}	N_0, m^{-3}	d, nm	H, nm	α_i	d_g, nm	d_{ch}, nm	γ_c,	D	m	M
80000	0.4	40	60	10^{-10}	5×10^{22}	8	8	0.1	8000	210	52%	16	2.7	0.16

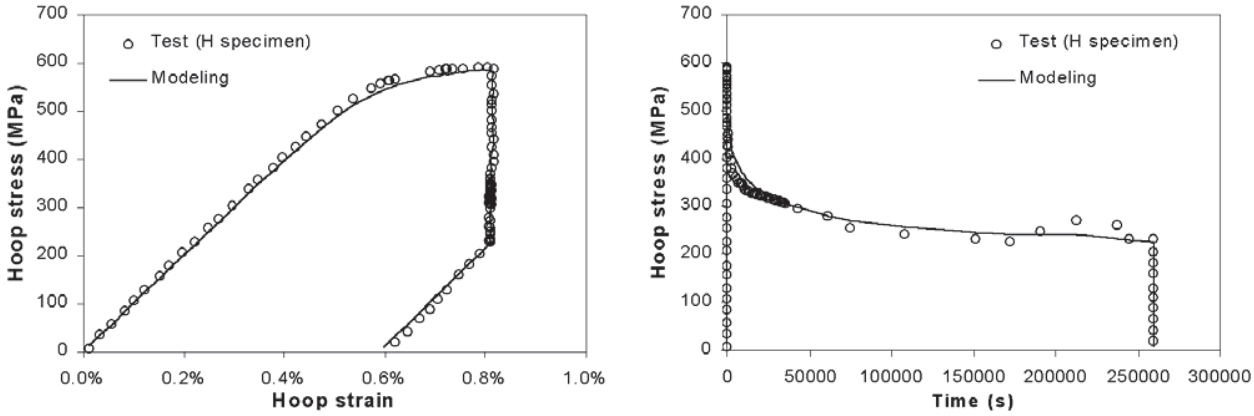

(a) (b)

FIG. 10—*(*a*) and (*b*) test simulation performed with the modeling compared to the mechanical test carried out on the H specimen.*

Discussion

Taking explicitly into account the strain localization in the channels, the model is able to reproduce the high strain hardening rate observed at the beginning of the plastic flow due to the strong internal stress, the saturation of the strain hardening rate, and also the high stress relaxation. However, three empirical fitting parameters (*D*, *M*, and *m*) are used for this modeling leading to a limited prediction capability. It also has to be underlined that by taking the shape and the orientation of the channels into account in a homogenization model, several assumptions and simplified hypotheses have to be made. Moreover, this approach does not use a self-consistent scheme, from the homogenization theory point of view, contrary to the modeling developed for non-irradiated material [1,2,34–37]. Other types of modeling are currently being studied in order to overcome these limitations.

Conclusions

The statistical TEM investigation has shown, thanks to numerous observations, that for transverse tensile tests and internal pressure tests performed at 350°C and up to the uniform elongation limit, only basal channeling occurs, whereas for non-irradiated material tested in the same conditions, only prismatic systems are activated. This change in the principal slip system with irradiation is believed to be due to the fact that the junctions created between dislocations and loops are always glissile for dislocations gliding in the basal plane, whereas it is sessile (in two cases over three) for dislocations gliding in the prismatic plane. However, it has been shown that for an axial tensile test, since basal planes are not well orientated with respect to the loading

direction. Considering the strong texture of the material, other slip systems are activated in order to accommodate the plastic strain. Thus, prismatic and pyramidal channeling occurs by means of other mechanisms for this loading direction, and no basal channels can be seen. It has also been shown that for transverse tensile tests, basal channels propagate from grain to grain in the shearing direction in order to accommodate the strong stress concentration created on grain boundaries.

The extension to other test conditions using a qualitative TEM analysis has shown that for lower strain rate (3×10^{-6} s^{-1}) deformation still occurs via basal channeling. However, for creep tests performed at 350°C during 500 h at a stress of 300 MPa, the irradiation microstructure starts to recover, leading to homogeneous like deformation zones. Nevertheless, basal channels can still be observed. Finally, it has been shown that for test performed at 400°C (during 72 h), the irradiation microstructure has been partially annealed, leading to homogeneous deformation at the grain scale probably occurring by prismatic glide. It has also been shown that for strain levels higher than the uniform elongation limit measured in transverse tensile loading, prismatic and pyramidal channels start to appear (in addition to the basal channels already present in the material) in order to accommodate the plastic strain in the necking zone.

The role of the dislocation channeling mechanism on the macroscopic mechanical behavior has been investigated by comparing the strain hardening behavior in internal pressure test at 350°C to TEM observations. It is proposed that the strong localization of the plastic deformation at the grain scale, in channels, as well as the occurrence of only basal slip, induces high internal stresses which compensate the local softening in the channels. As a consequence, it is proposed that an important part of the macroscopic flow stress is due to the kinematic hardening associated with the development of the internal stresses. It is also proposed that the high hardening rate at the onset of plastic flow is due to the low volume fraction of channels that deforms plastically. The saturation of the flow stress is assumed to be linked to the propagation of channels to surrounding grains due to high local stress concentration.

A micro-mechanical modeling has been developed to take into account the dislocation channeling process. The loop-dislocation interaction has been simply modeled at the dislocation scale, taking into account the dispersed barrier hardening due to the high density of <a> loops and the softening due to loop sweeping up inside the channels. Then, at the grain scale the channels' microstructures have been schematically described, in order to use homogenization techniques, taking explicitly into account the shape, the orientation, and the volume fraction of the channel inside the grains. Finally, a polycrystalline model has been adapted to irradiated material, using simple assumptions and simple approaches, in order to model the behavior of the material at the macroscopic scale. This model is able to reproduce the strong strain hardening, the saturation of the strain hardening, as well as the stress relaxation. Nevertheless, further developments are needed in order to avoid the introduction of the image stress [33] and the use of fitting parameters.

References

[1] Geyer, P., Feaugas, X., and Pilvin, P., "Modeling of the Anisotropic Viscoplastic Behavior of Fully Annealed Zircaloy-4 Tubes by a Polycrystalline Approach," *Plasticity '99*, Cancun, January 1999.

[2] Brenner, R., Béchade, J. L., Castelnau, O., and Bacroix, B., "Thermal Creep of Zr-Nb1%-O Alloys: Experimental Analysis and Micromechanical Modeling," *J. Nucl. Mat.*, Vol. 305, 2002, pp. 175–186.

[3] Douglass, D. L., "The Metallurgy of Zirconium," *Atomic Energy Review supplement*, International Atomic Energy Agency, 1971.
[4] Northwood, D. O., Gilbert, R. W., Bahen, L. E., Kelly, P. M., Blake, R. G., Jostsons, A., et al., "Characterization of Neutron Irradiation Damage in Zirconium Alloys - An International Round-Robin Experiment," *J. Nucl. Mat.*, Vol. 79, 1979, pp. 379–394.
[5] Bement, A. L., "Fundamental Materials' Problems in Nuclear Reactors," Second International Conference on the Strength of Metals and Alloys, ASM, Metals Park, OH, Vol. 2, 1970, pp. 693–728.
[6] Hirsch, P. B., "Point Defect Cluster Hardening," *Proceedings of a Conference on Point Defect Behavior and Diffusional Processes*, University of Bristol, 13–16 September 1976.
[7] Wechsler, M. S., "Dislocation Channeling in Irradiated and Quenched Metals, The Inhomogeneity of Plastic Deformation," ASM, Metals Park, OH, 1973, pp. 19–52.
[8] Coleman, C. E., Mills, D., van der Kuur, J., "Deformation Parameters of Neutron Irradiated Zy-4 at 300°C," *Canadian Metallurgical Quaterly*, Vol. 11, 1972, pp. 91–100.
[9] Onchi, T. Kayano, H., Higashiguchi, Y., "The Inhomogeneous Deformation Behavior of Neutron Irradiated Zircaloy-2," *J. Nucl. Mat.*, Vol. 88, 1980, pp. 226–235.
[10] Williams, C. D., Adamson, R. B., and Olhausen, K. D., "Effects of Boiling Water Reactor Irradiation on Tensile Properties of Zircaloy," *European Conference on Irradiation Behavior of Fuel Cladding and Core Component Materials*, Karlsruhe, 1974, pp. 189–192.
[11] Pettersson, K., "Evidence for Basal or Near-Basal Slip in Irradiated Zircaloy," *J. Nucl. Mat.*, Vol. 105, 1982, pp. 341–344.
[12] Adamson, R. B. and Bell, W. L., "Effects of Neutron Irradiation and Oxygen Content on the Microstructure and Mechanical Properties of Zircaloy, Microstructure and Mechanical behavior of materials," Vol. 1, International Symposiums, Xian, China, 1985, pp. 237–246.
[13] Fregonese, M., Régnard, C., Rouillon, L., Magnin, T., Lefebvre, F., and Lemaignan, C., "Failure Mechanisms of Irradiated Zr Alloys Related to PCI: Activated Slip Systems, Localized Strains, and Iodine-Induced Stress Corrosion Cracking," *Zirconium in the Nuclear Industry: 12th International Symposium, ASTM STP 1354*, ASTM International, West Conshohocken, PA, 2000, pp. 377–398.
[14] Régnard, C., Verhaeghe, B., Lefebvre-Joud, F., and Lemaignan, C., "Activated Slip Systems and Localized Straining of Irradiated Alloys in Circumferential Loadings," *Zirconium in the Nuclear Industry, 13th International Symposium, ASTM STP 1423*, ASTM International, West Conshohocken, PA, 2002, pp. 384–399.
[15] Odette, G. R., He, M. Y., Donahue, E. G., Spätig, P., and Yamamoto, T., "Modeling of Multiscale Mechanics of Flow Localization-Ductility Loss in Irradiation Damaged bcc Alloys," *J. Nucl. Mat.*, Vols. 307–311, 2002, pp. 171–178.
[16] Gilbon, D., Soniak, A., Doriot, S., and Mardon, J.-P., "Irradiation Creep and Growth Behavior, and Microstructural Evolution of Advanced Zr-Base Slloys," *Zirconium in the Nuclear Industry: 12th International Symposium, ASTM STP 1354*, ASTM International, West Conshohocken, PA, 2000, pp. 51–73.
[17] Desquines, J. B., Desquines, J., Cazalis, B., Bernaudat, C., Poussard, C., Averty, X., et al., "Mechanical Properties of Zircaloy-4 PWR Fuel Cladding with Burnup 60–64 MWd/kgU and Implications for RIA Behavior," *Zirconium in the Nuclear Industry: 14th International Symposium*, ASTM International, West Conshohocken, PA, to be published.

[18] Gilbon, D. and Simonot, C., "Effect of Irradiation on the Microstructure of Zircaloy-4," *Zirconium in the Nuclear Industry: 10th International Symposium, ASTM STP 1245*, ASTM International, West Conshohocken, PA, 1994, pp. 521–548.
[19] Onimus, F., Monnet, I., Béchade, J. L., Prioul, C., and Pilvin, P., "A Statistical TEM Investigation of Dislocation Channeling Mechanism in Neutron Irradiated Zirconium Alloys," *Journal of Nuclear Materials*, Vol. 328, 2004, pp. 165–179.
[20] Tenckhoff, E., "Deformation Mechanisms, Texture, and Anisotropy in Zirconium and Zircaloy," *ASTM STP 966*, ASTM International, West Conshohocken, PA, 1988, pp. 1–34
[21] Carpenter, G. J. C., "Dislocation Channeling by Prism Slip in HCP Metals," *Scripta. Metall.*, Vol. 10, 1976, p. 411.
[22] Ferrer, F., Barbu, A., Bretheau, T., Crépin, J., Willaime, F., and Charquet, D., "The Effect of Small Concentrations of Sulfur on the Plasticity of Zirconium Alloys at Intermediate Temperatures," *Zirconium in the Nuclear Industry, 13th Symposium, ASTM STP 1423*, 2002, pp. 863–887.
[23] Higgy, H. R. and Hammad, F. H., "Effect of Neutron Irradiation on the Tensile Properties of Zy-2 and Zy-4," *J. Nucl. Mat.*, Vol. 44, 1972, pp. 215–227.
[24] Baroch, C. J., "Effect of Irradiation at 130, 650, and 775°F on Tensile Properties of Zy-4 at 72, 650, and 775°F," *Properties of Reactor Structural Alloys after Neutron or Particle Irradiation, ASTM STP 570*, ASTM International, West Conshohocken, PA, 1975, pp. 129–242.
[25] Yasuda, T., Nakatsuka, M., and Yamashita, K., "Deformation and Fracture Properties of Neutron-Irradiated Recrystallized Zircaloy-2 Cladding under Uniaxial Tension," *Zirconium in the Nuclear Industry: 7th International Symposium, ASTM STP 939*, ASTM International, West Conshohocken, PA, 1987, pp. 734–747.
[26] Brown, L. M. and Ham, R. K., "Strengthening Methods in Crystals," Applied Science Publishers Ltd., K. A. Nicholson, Ed., 1971, pp. 9–135.
[27] Rieger, G. F. and Lee, D., "Strength and Ductility of Neutron Irradiated and Textured Zy-2," *Zirconium in Nuclear Applications, ASTM STP 551*, ASTM International, West Conshohocken, PA, 1974, pp. 355–369.
[28] Rodney, D., Martin, G., and Bréchet, Y., "Irradiation Hardening by Interstitial Loops: Atomistic Study and Micromechanical Model," *Materials Science and Engineering*, A309–310, 2001, pp. 198–202.
[29] Pokor, C., "Effect of Irradiation Defects on the Work Hardening Behavior," *Scripta Materialia*, Vol. 50, 2004, pp. 597–600.
[30] Friedel, J., "Dislocations," Pergamon Press, 1964.
[31] Cagnon, M., "Thermodynamique de la déformation et essais mécaniques – Théorie de l'activation thermique," Ecole d'été d'Yravals, Dislocations et déformation plastique, Groh P., Kubin L.P., Martin, J.L., Eds., Les Editions de Physique, 1979, pp. 53–66.
[32] Eshelby, J. D., "The Determination of the Elastic Field of an Ellipsoidal Inclusion, and Related Problem," *Proc. R. Soc. Lond.*, A241, 1957, pp. 376–396.
[33] Mura, T, "Micromechanics of Defects in Solids," Martinus Nijhoff Publishers, The Hague, 1982, pp. 63–70.
[34] Pilvin, P., "The Contribution of Micromechanical Approaches to the Modelling of the Inelastic Behaviour of Polycrystals," *Proc. Int. Conf. on Biaxial/Multiaxial Fatigue ESIS/SF2M*, 1994, pp. 31–46.

[35] Lebenshon, R. A. and Tomé, C.N.,"A Self-Consistent Anisotropic Approach for the Simulation of Plastic Deformation and Texture Development of Polycrystals: Application to Zirconium Alloys," *International Journal of Plasticity*, Vol. 11, No. 3, 1995, pp. 1881–1890.
[36] Turner, P. A., Christodoulou, N., and Tomé, C. N., "Modeling the Mechanical Response of Rolled Zircaloy-2," *International Journal of Plasticity*, Vol. 11, No. 3, 1995, pp. 1881–1890.
[37] Berveiller, M. and Zaoui, A., "An Extension of the Self-Consistent Scheme to Plastically-Flowing Polycrystals," *J. Mech. Phys. Solids*, Vol. 26, 1979, pp. 325–344.
[38] Mills, D. and Craig, G. B., "The Plastic Deformation of Zirconium-Oxygen Alloy Single Crystals in the Range 77–950 K," *Trans. of Metall. Society of AIME*, Vol. 242, 1968, pp. 1881–1890.
[39] Conrad, H., "Effect of Interstitial Solutes on the Strength and Ductility of Titanium," *Progress in Material Science*, Vol. 26, 1981, pp. 123–403.
[40] Akhtar, A., "Basal Slip in Zirconium," *Acta. Metall.*, Vol. 21, 1973, pp. 1–11.